Volume 7 | Number 14 | 14 April 2019 | Pages 7941–8654

Journal of Materials Chemistry A

Materials for energy and sustainability

rsc.li/materials-a

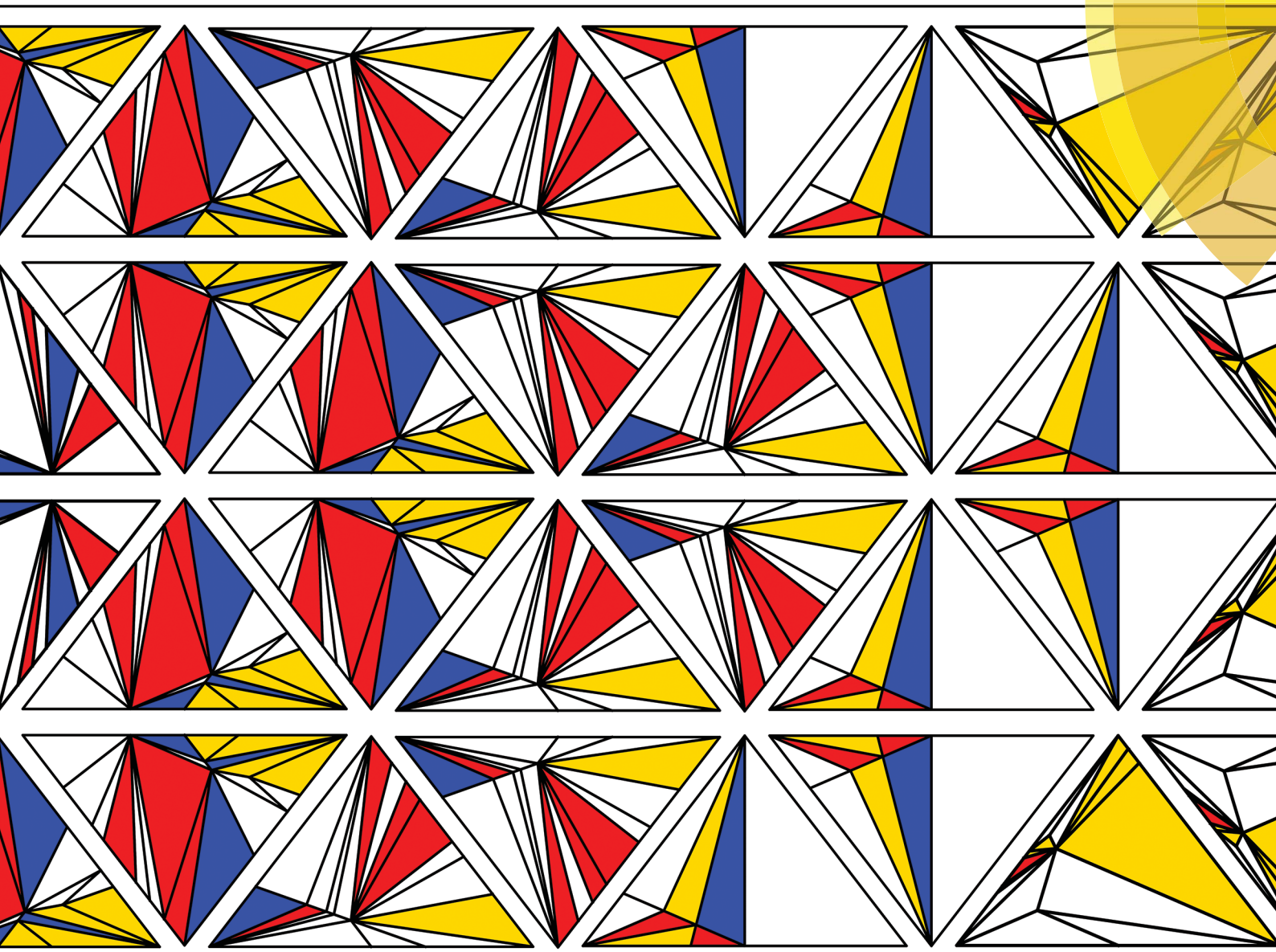

ISSN 2050-7488

ROYAL SOCIETY OF CHEMISTRY | Celebrating IYPT 2019

PAPER

Valentina Lacivita, Gerbrand Ceder *et al.*

Ab initio investigation of the stability of electrolyte/electrode interfaces in all-solid-state Na batteries

Journal of Materials Chemistry A

PAPER

View Article Online
View Journal | View Issue

Cite this: J. Mater. Chem. A, 2019, 7, 8144

Ab initio investigation of the stability of electrolyte/electrode interfaces in all-solid-state Na batteries†

Valentina Lacivita, *[a] Yan Wang, [b] Shou-Hang Bo[c] and Gerbrand Ceder*[ad]

All-solid-state batteries show great potential for achieving high energy density with less safety problems; however, (electro)chemical issues at the solid electrolyte/electrode interface may severely limit their performance. In this work, the electrochemical stability and chemical reactivity of a wide range of potential Na solid-state electrolyte chemistries were investigated using density functional theory calculations. In general, lower voltage limits are predicted for both the reduction and oxidation of Na compounds compared with those of their Li counterparts. The lower reduction limits for the Na compounds indicate their enhanced cathodic stability as well as the possibility of stable sodium metal cycling against a number of oxides and borohydrides. With increasing Na content (or chemical potential), improved cathodic stability but also reduced anodic stability are observed. An increase in the oxidation voltage is shown for Na polyanion systems, including borohydrides, NaSICON-type oxides, and aluminates, due to the covalent stabilization of the anions. In addition, the oxides exhibit remarkable chemical stability when in contact with various cathode materials (layered transition metal oxides and fluorophosphates), whereas the chalcogenides predictably display narrow electrochemical windows and high chemical reactivity. Our findings indicate some promising candidates for solid-state conductors and/or protective coating materials to enable the operation of high-energy-density all-solid-state Na batteries.

Received 1st November 2018
Accepted 4th January 2019

DOI: 10.1039/c8ta10498k

rsc.li/materials-a

1 Introduction

The increasing demand for rechargeable batteries that deliver high energy density without safety hazards is driving the development of all-solid-state batteries (SSBs), in which liquid electrolytes are replaced by solid alkali conductors. Research in this field has led to the discovery of numerous solid electrolytes with room-temperature (RT) ionic conductivities of up to 10–20 mS cm^{-1}, which are comparable or even superior to those of common liquid electrolytes. These promising solid electrolytes include NaSICON-type oxides,[1,2] garnets,[3,4] and thiophosphates, such as $Li_{10}GeP_2S_{12}$ (ref. 5) and $Li_7P_3S_{11}$ (ref. 6) for lithium batteries, and Na_3PS_4 (ref. 7) and Na_3PSe_4 (ref. 8) for sodium batteries.

However, the high resistivity at the electrolyte/electrode interface severely limits the power and rate capabilities of SSBs. This high internal resistivity is attributed to chemical and/or electrochemical compatibility issues at the interface as well as mechanical issues (*e.g.*, poor interfacial contact and volume changes). Examples of electrode/solid electrolyte combinations undergoing interfacial reactions include $LiCoO_2/Li_2S$–P_2S_5 (ref. 9) and $LiCoO_2/Li_7La_3Zr_2O_{12}$,[10] and their interfaces have been characterized using transmission electron microscopy. First-principles density functional theory (DFT) calculations have proven to be a valuable tool for the systematic investigation of the (electro)chemical compatibility at electrode/electrolyte interfaces.[11–13] DFT-computed 0 K phase diagrams can be used to derive the phase equilibria at the interface and to estimate the driving force for interface reactions and electrolyte decomposition when an external potential is applied.

Richards *et al.*[12] and Zhu *et al.*[11,13] have applied this computational approach to a number of electrolyte/electrode (and coating/cathode) interfaces relevant for all-solid-state lithium batteries. Contrary to the common belief that solid-state electrolytes have high intrinsic stability, they demonstrated that many electrolyte/electrode combinations display quite limited chemical and electrochemical compatibility. In most cases, an interface layer with multiple decomposition phases was predicted to form at the electrode/electrolyte contact. This interlayer, however, can be beneficial for the system stability if it is both ion-conducting and passivating. In this case, the interlayer acts as an electronic insulator, bridging

[a]Materials Sciences Division, Lawrence Berkeley National Laboratory, Berkeley, CA 94720, USA. E-mail: vlacivita@lbl.gov; gceder@berkeley.edu
[b]Advanced Materials Lab, Samsung Research America, 3 Van de Graaff Drive, Burlington, MA 01803, USA
[c]University of Michigan—Shanghai Jiao Tong University Joint Institute, Shanghai Jiao Tong University, 800 Dong Chuan Road, Minhang District, Shanghai 200240, China
[d]Department of Materials Science & Engineering, University of California Berkeley, Berkeley, CA 94720, USA

† Electronic supplementary information (ESI) available. See DOI: 10.1039/c8ta10498k

the difference in the chemical potentials μ of all the atomic species between the electrolyte and electrodes.

Beyond a purely thermodynamic model, kinetic barriers for decomposition and chemical reactions may intervene to widen the effective voltage stability window of the electrolyte and possibly change the constitution of the interphase layer at the electrolyte/cathode interface. An estimate of the upper kinetic voltage limit for the electrolyte decomposition can be obtained by calculating the voltage corresponding to the topotactic extraction of an atom of the mobile species, as proposed by Tian *et al.*[14] These authors used a combination of DFT calculations and experiments to investigate the electrochemical stability of Na_3PX_4 (X = S, Se) solid electrolytes and their compatibility with various layered transition metal (TM) oxide cathodes for sodium-ion batteries. They verified that the anodic voltage limit measured for the electrolytes always lies between the computed thermodynamic upper bound and the potential for topotactic desodiation. Moreover, they reported evidence for electrolyte/cathode reactions for which the formation of intermediate products is kinetically favored over stable thermodynamic phases. One example is the Na_3PS_4–$NaCrO_2$ interface, for which they observed the formation of Na_3PS_3O at temperatures below 500 °C instead of the predicted products Na_3PO_4 and $NaCrS_2$. More recently, Tang *et al.*[15] applied finite-temperature *ab initio* molecular dynamics simulations to assess kinetic effects on the interface reactivity. They observed that contrary to thermodynamic models predicting the formation of stable $[PO_4]^{3-}$ groups *via* anion-exchange reactions, the formation of $[SO_4]^{2-}$-containing compounds and Na_3P is kinetically favored. In the same study, the authors also calculated the electrochemical stability and chemical reactivity of some well-known Na solid-state electrolytes with different cathode, anode, and buffer materials.

In this work, we aim to extend previous computational surveys on solid-state Na conductors[14,15] to provide a systematic and comprehensive overview of promising electrolyte/electrode and coating/electrode combinations for Na SSBs. We apply the computational approaches described in ref. 11–14 to estimate the electrochemical stability window of numerous solid-state electrolyte candidates, the kinetic voltage limits for Na extraction, and the chemical reactivity with different cathode materials. We investigate an extensive selection of materials, including known Na-ion conductors and possible decomposition or reaction products as well as possible coating layers. In addition, a comparison with relevant Li compounds is performed. In line with previous assessments,[14,15] we confirm general trends such as the greater electrochemical stability of oxides than that of sulfides/selenides and the existence of a large thermodynamic driving force for anion-exchange reactions between thiophosphates and layered TM oxide cathodes. Moreover, we show that sodium electrolytes generally exhibit improved cathodic (low-voltage) stability compared with their lithium analogues, thus giving prospects for the stable cycling of Na metal anodes. We find that the differences between sodium and lithium compounds in anodic (high-voltage) limits are not simply deducible from the electrochemical scale, but also relate to structural factors, such as the cation–anion radius ratio. Both the thermodynamic and kinetic upper voltage limits of compounds are favorably extended by covalent stabilization in polyanions such as phosphates and boranes, which emerge as materials that can tolerate charging potentials as high as 4–5 V.

2 Methods

In the current work, we adopt the methodology described in ref. 12,16, and 17. We consider three different indicators of the stability of the solid-state electrolyte: (1) the pure thermodynamic voltage stability *versus* the metal anode (M), (2) the upper kinetic voltage limit for the extraction of one alkaline atom from the solid-state electrolyte, and (3) the chemical reactivity at the electrolyte/cathode interface.

2.1 Voltage window and interface chemical stability

Phase diagrams were constructed using the Python Materials Genomics (pymatgen) library[18] and a dataset of energies from DFT relaxation of compounds initialized using structural information obtained from the Inorganic Crystal Structure Database (ICSD)[19] or structures generated by a data-mined chemical substitution algorithm[20] (see Table S1 of the ESI† for more details). DFT calculations were performed using the generalized gradient approximation (GGA) to the exchange–correlation functional in the Perdew–Burke–Ernzerhof formulation,[21] as implemented in the Vienna *Ab initio* Simulation Package (VASP),[22] within the projector-augmented wave formalism.[23] The energy cutoff was set to 520 eV, and a *k*-point grid with a density of at least 500/(number of atoms) was used for all the computations. For compounds containing TM elements with localized d electrons, the GGA + U variation[24] of the density functional was adopted. Consistency across GGA and GGA + U calculations is maintained by the application of the mixing scheme as described in ref. 25. Moreover, GGA errors of reaction energies involving gas/liquid phase molecules were corrected using Wang *et al.*'s method.[26] Following Richards *et al.*,[12] the formation energies were calculated from the nearest phases (*i.e.*, the phases that define the low energy facet containing the target composition in the phase diagram) for which the experimental energies are available in the Kubaschewski[27] or NIST-JANAF[28] thermochemical tables. For example, the formation energy of $NaZr_2(PO_4)_3$, a compound not listed in the thermochemical tables, is calculated as the DFT energy of the reaction $2ZrO_2 + P_2O_5 + NaPO_3 \rightarrow NaZr_2(PO_4)_3$, to which are added the experimental formation energies of ZrO_2, P_2O_5 and $NaPO_3$. Such an approach allows benefitting from the higher accuracy of DFT reaction energies that are calculated between compounds whose elements are in the same oxidation states.[29] If no experimental data are available for some nearest phases, the corresponding elemental precursors are used for reference.

2.1.1 Thermodynamic stability window of the solid-state electrolyte. The voltage stability window of a compound is calculated from its grand potential phase diagram. The window is defined as the range of M chemical potentials (μ_M) over which each electrolyte is predicted to be stable, that is, when its grand potential

$$\Phi(c,\mu_M) = E(c) - n_M(c)\mu_M \quad (1)$$

lies on the lowest surface of the optimized convex energy hull for the chemical system. Here, $E(c)$ and $n_M(c)$ represent the DFT energy and concentration of the alkali metal, respectively, at the relevant composition c. The highest (lowest) chemical potential at which the electrolyte is stable is the cathodic (anodic) limit of the electrolyte.[12]

2.1.2 Kinetic upper voltage limit of the solid-state electrolyte. In addition to the thermodynamic stability window defined in Section 2.1.1, the maximum kinetic voltage limit for a solid-state conductor can be defined as the potential at which one alkali ion M^+ and one electron e^- are extracted, *i.e.*,

$$\Delta V = -(E_{def} - E_0 - \mu_M), \quad (2)$$

where E_0 and E_{def} are the DFT bulk energies after structural relaxation of the pristine and defected compound, respectively.[14] As both the extractions of M^+ and e^- are fast processes, it is unlikely that this voltage limit can be exceeded without rapid breakdown of the solid electrolyte. E_{def} is calculated at the supercell size convergence to ensure negligible interactions between defect images.

2.1.3 Chemical reactivity of the solid-state electrolyte with the cathode. The stability of the electrolyte/cathode interface is determined from the phase diagram of their combined chemistry, by considering the reaction (if any) between the electrode and electrolyte with the highest calculated driving force,[12] namely

$$\Delta E(c_a, c_b) = \min_{x\in[0,1]} \{E_{pd}(xc_a + (1-x)c_b) - xE_{pd}(c_a) - (1-x)E_{pd}(c_b)\} \quad (3)$$

In the above equation x is the mixing fraction of the electrode and electrolyte compositions, c_a and c_b, respectively; $E_{pd}(c_a)$ and $E_{pd}(c_b)$ are the respective convex hull minimum energies; and $E_{pd}(xc_a + (1-x)c_b)$ is the convex hull function returning the lowest energy equilibrium of the phases at the given composition.

2.2 Materials selection

Solid-state electrolyte (or coating) candidates were selected based on their Na content and electrochemical performance, as reported in the literature. We focused particularly on known solid-state Na-ion conductors with high ionic conductivity or with the potential for high ionic conductivity.

2.2.1 Aluminates. Na-β-alumina, $(1+x)Na_2O\cdot 11Al_2O_3$, has been known as a solid-state Na-ion conductor for 50 years[30] and was critical in the development of Na–S and (ZEBRA) batteries,[31–34] which operate above 300 °C. In addition to the hexagonal ($P6_3/mmc$) β form ($NaAl_{11}O_{17}$),[35] a rhombohedral ($R\bar{3}mH$) β″ form ($Na_{1.67}Al_{11}O_{17}$), has also been characterized.[36] The latter exhibits a higher conductivity ($\sigma \approx 2$ mS cm^{-1} at RT) and has been proven to be stable against Na.[37]

For comparison, we also considered the stability of $NaAlO_2$ and of the Na-rich aluminates Na_5AlO_4, $Na_7Al_3O_8$, $Na_{14}Al_4O_{13}$, and $Na_{17}Al_5O_{16}$.[38] $NaAlO_2$ is a side product in β-alumina mixtures and has been used as a cathode coating material on $LiCoO_2$.[39] To our knowledge, no data on the ionic conductivity and stability window of the Na-rich aluminates have been reported yet.

2.2.2 NaSICONs. The Na Super Ion CONductor (NaSICON) class of materials, $Na_{1+x}Zr_2Si_xP_{1-x}O_{12}$ ($0 \le x \le 3$), was first introduced in 1976[40,41] as the outcome of a search for structures with fast alkali-ion transport. Because of their compositional diversity, these materials are very attractive in battery applications not only as solid electrolytes but also as electrodes.[42] Their conductivity can reach levels of 10^{-3} S cm^{-1} at RT;[43] however, NaSICONs suffer from large interfacial impedance and Na dendrite propagation, though promising solutions have recently been proposed.[44] Degradation of NaSICON ceramics by molten Na has been observed for P-containing compositions in static corrosion tests, whereas the pure silicates appear to be kinetically stabilized.[45]

2.2.3 Antiperovskites and other oxides. Na_3OBr and Na_4OI_2 have cubic ($Pm\bar{3}m$) and tetragonal ($I4/mmm$) antiperovskite structures, respectively. Recently, Zhu *et al.*[46] analyzed their Na-ion transport mechanisms and reported low ionic conductivities ($\sigma \approx 10^{-8}$ S cm^{-1} at RT, activation energy $E_a = 0.6$–0.7 eV). Nonetheless, chemical modifications leave substantial room for improvement, *e.g.*, by aliovalent substitution the conductivity of $Na_{2.9}Sr_{0.05}OBr_{0.6}I_{0.4}$ reaches 0.19 mS cm^{-1} at 200 °C.[47]

Other oxides such as Na_2SO_4, Na_3PO_4, and Na_4SiO_4, are generally characterized by low ionic conductivity. However, they can be used as coating materials or end-members of better performing electrolyte solid-solutions such as Na_2SO_4/Na_4SiO_4,[48] Na_3PO_4/Na_2SO_4,[49,50] Na_3AlF_6/Na_2SO_4,[50] and Na_3PO_4/Na_4SiO_4.[51]

2.2.4 Sulfides and selenides. Na_3PS_4 has been known as a Na-ion conductor for more than 25 years[52] and has garnered renewed research interest since Hayashi *et al.*[7] reported a glass–ceramic phase containing cubic Na_3PS_4 with $\sigma = 2 \times 10^{-4}$ S cm^{-1}. Similar RT ionic conductivity has been reported for the isostructural selenide compound Na_3PSe_4.[8] One major issue with the use of Na_3PS_4 and Na_3PSe_4 as solid electrolytes is their instability against Na metal, as they decompose into Na_2S/Na_2Se + Na3P forming a resistive interphase that grows in time.[14,37] Glass–ceramic electrolytes exhibit even higher Na^+ conductivities (7.4×10^{-4} S cm^{-1} at RT), and cyclic voltammetry suggests they have remarkable electrochemical stability.[53] Tetragonal Na_3SbS_4 has also been described as a highly conductive phase ($\sigma > 1.1$ mS cm^{-1} at RT) stable in dry-air.[54] Finally, the computation-assisted discovery of tetragonal $Na_{10}SnP_2S_{12}$ with a RT ionic conductivity of 0.4 mS cm^{-1} ($E_a = 0.365$ eV) and improved processability with respect to β-alumina and NaSICON compounds was recently reported.[55]

2.2.5 Borohydrides. Superionic conduction in alkali metal borohydrides is commonly associated with the thermally activated orientational disorder of the $[B_xH_y]^-$ anions. Impedance measurements[56] indicate exceptionally high Na^+ conductivity in $Na_2B_{12}H_{12}$ (on the order of 0.1 S cm^{-1}) above its order-to-disorder (monoclinic-to-cubic) phase transition at approximately 529 K. Similar electrochemical behavior was also

observed for $LiBH_4$, where raising the temperature to approximately 390 K induces an orthorhombic-to-hexagonal phase change signaled by a dramatic increase in σ to 10^{-3} S cm^{-1}.[57] Despite its high conductivity and good compatibility with Li metal, $LiBH_4$ is easily oxidized by metal oxide cathodes and thus requires coating to avoid large interfacial resistance and consequent capacity loss.[58] The sodiated analogue, $NaBH_4$, also undergoes an order-to-disorder phase transition (from tetragonal to cubic) at temperatures above 190 K.[59] The much lower transition temperature of $NaBH_4$ compared to $Na_2B_{12}H_{12}$ supports the observation by Lu and Ciucci[60] that the rotation barrier for $[B_xH_y]^-$ anions correlates positively with the anion size so that RT superionic conduction could be pursued by anion mixing.

2.2.6 Halo-aluminates. $NaAlCl_4$ is generally used as a catholyte (*i.e.*, a molten salt secondary electrolyte) along with β-alumina in ZEBRA batteries.[61,62] Similarly, molten eutectic mixtures of Na haloaluminate salts, $NaAlX'_{4-\delta}X''_{\delta}$ (with $0 < \delta < 4$ and $X'/X'' = Cl, Br, I$), have been used as electrolytes in the cathode composite to enable operation of molten Na metal halide batteries at substantially lower temperatures compared with the traditional ZEBRA system.[63] The aluminum fluorides Na_3AlF_6 (cryolite) and $Na_5Al_3F_{14}$ (chaolite) exhibit fast Na-ion diffusion at high temperatures as revealed by nuclear magnetic resonance measurements.[64,65]

2.2.7 Binaries. In addition to the materials listed above we will also discuss simple alkali binaries. By comparing Na and Li binaries with identical structures we can show how a good match of structure type with ion size enhances the anodic stability of a solid.

3 Results

3.1 Comparison of the electrochemical stability window of Na and Li binaries

Fig. 1 compares the stability windows of simple Na binary compounds with those of their Li analogues. Although these compounds may not be considered solid-electrolyte candidates by themselves due to their generally poor ionic conductivity (except for Li_3P[66]), it is instructive to compare their electrochemical stability as a basis to understand the behavior of more complex compounds. These binaries are generally used as synthesis precursors, *e.g.*, M_2S or M_2Se in chalcogenide-based glassy electrolytes, or as additives (especially the halides) to improve the electrochemical performance of more complex electrolyte materials.[67–70] In all of these binary materials, the anion is fully reduced; therefore, further reaction with the metal anode cannot occur and they are all stable down to 0 V against M/M^+.

The RT crystal structures of the Na and Li binaries are isomorphic (see Table 1), which ensures that the differences in the thermodynamic voltage stability windows are exclusively due to differences in the chemistry. Indeed, all the hydrides, halides, and chalcogenides have a face-centered cubic structure ($Fm\bar{3}m$) with M^+ cations located in octahedral or tetrahedral sites depending on whether they are 1 : 1 (rock-salt) or 2 : 1 (anti-fluorite) binaries, respectively. The phosphides, instead, have both a hexagonal structure.

For simple binaries, such as MF, MCl, MBr, and MI, the anodic decomposition is into the elements and this creates a direct relationship between the formation enthalpy of the compound, ΔH, and the anodic voltage limit: $\Delta H \approx -V$. As Table 1 shows, the anodic stability of Na binaries is generally lower than that of Li binaries. This trend might be expected from the fact that the standard reduction potential for the reaction $Na^+(aq) + e^- \rightarrow Na(s)$ is 0.33 V above that of Li, although reference to half-cell reduction potentials, which are dependent on the solvent and solute concentration, is not rigorously applicable.[72] The exceptions to this trend are pairings with large anions such as Cl^-, Br^-, and I^-, where the reduced size mismatch with Na^+ plays a stabilizing role compared to the equivalent Li binaries. Such stabilization of the Na compounds with large anions, as compared to their Li equivalents, is confirmed by the experimental formation enthalpies in Table 1. We attribute this stabilization to the better match of the Na^+ radius with those of the large halogen anions. In simple high-symmetry crystal structures, such as the rock-salt structure of these compounds, the lattice constant is the only geometric

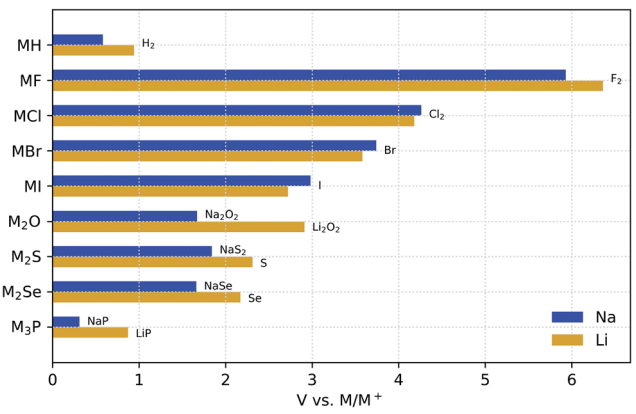

Fig. 1 Electrochemical stability window of Na and Li binary compounds. The oxidation products are shown at the anodic limits.

Table 1 Space group (SG) of the most stable Na and Li binary entries in the database, calculated cell voltages, V^0_{calc} (V), and experimental RT formation enthalpies, ΔH^f_{exp} (eV). The formation enthalpy for Na_2Se is from ref. 71 all the other experimental data are from ref. 27 and 28

	M = Na			M = Li		
	SG	V^0_{calc}	ΔH^f_{exp}	SG	V^0_{calc}	ΔH^f_{exp}
MH	$Fm\bar{3}m$	0.58	−0.58	$Fm\bar{3}m$	0.94	−0.94
MF	$Fm\bar{3}m$	5.93	−5.94	$Fm\bar{3}m$	6.36	−6.39
MCl	$Fm\bar{3}m$	4.26	−4.26	$Fm\bar{3}m$	4.18	−4.23
MBr	$Fm\bar{3}m$	3.74	−3.74	$Fm\bar{3}m$	3.58	−3.64
MI	$Fm\bar{3}m$	2.98	−2.98	$Fm\bar{3}m$	2.80	−2.80
M_2O	$Fm\bar{3}m$	1.67	−4.30	$Fm\bar{3}m$	2.91	−6.20
M_2S	$Fm\bar{3}m$	1.84	−3.80	$Fm\bar{3}m$	2.31	−4.64
M_2Se	$Fm\bar{3}m$	1.66	−3.44	$Fm\bar{3}m$	2.17	−4.36
M_3P	$P6_3/mmc$	0.31	—	$P6_3/mmc$	0.87	—

parameter that can be adjusted. When very small ions such as Li^+ are paired with large anions, such as Br^- and I^-, the difference in ionic radii creates a mismatch between anion–anion and cation–anion distances, which is, Fig. S1† shows the differences between the anodic voltages of Li and Na halides (ΔV) as a function of the anion radius.

Fig. 1 also shows that the nature of the oxidation products depends on the valence electron configuration of the anions. The oxidation of hydrides and halides yields their elementary references directly, whereas anions with higher valence (*e.g.*, O^{2-}, S^{2-}, and P^{3-}) usually transform into phases where the anion has an intermediate oxidation state. For example, both alkali oxides M_2O transform into peroxides M_2O_2 upon oxidation. However, although Li_2O_2 is known to be a fairly reactive species,[73,74] Na_2O_2 is a stable bulk phase in an oxygen atmosphere,[75] which may contribute to the reduction of the anodic limit of Na_2O with respect to that of Li_2O. Similarly to Na_2O, the Na chalcogenides oxidize to intermediate phases with partially oxidized anions that are stable at RT, *i.e.*, Na_2S_4 (ref. 76) and Na_2Se_2.[77] The Li chalcogenides lack these intermediate stable phases, which explains the direct oxidation of both Li_2S and Li_2Se to their elementary references at higher anodic voltages.

3.2 Electrochemical stability windows of Na solid-state electrolytes

3.2.1 Thermodynamic voltage limits. Using the selection criteria outlined in section 2.2, we calculated the electrochemical stability window of Na solid-state electrolyte candidates as shown in Fig. 2 along with some reference compounds. A complete list of the predicted oxidation and reduction reactions is provided in the supplementary Table S1.† For some of the selected compounds, namely $Na_{10}SnP_2S_{12}$, the NaSICONs $Na_3Zr_2(SiO_4)_2PO_4$ and $Na_4Zr_2(SiO_4)_3$, and the aluminates $NaAl_{11}O_{17}$ and $Na_{17}Al_5O_{16}$, the grand potential energy $\Phi(c,\mu_{Na})$ (eqn (1)) was never observed on the lowest surface of the phase diagram hull, indicating that they are metastable or high-temperature phases. Therefore, in these cases, the thermodynamic voltage stability window was evaluated by shifting the phase diagram hull by +25 meV/atom (the average thermal energy at RT). Note that such a shift is solely intended to make these compounds thermodynamic ground-states but does not modify the voltage limits in any meaningful way.

The sulfides and particularly the selenides display very narrow windows, which is in line with the relatively low electronegativity of the chalcogen anions and the versatility of their valence electron shell with oxidation states from −2 to +6. None

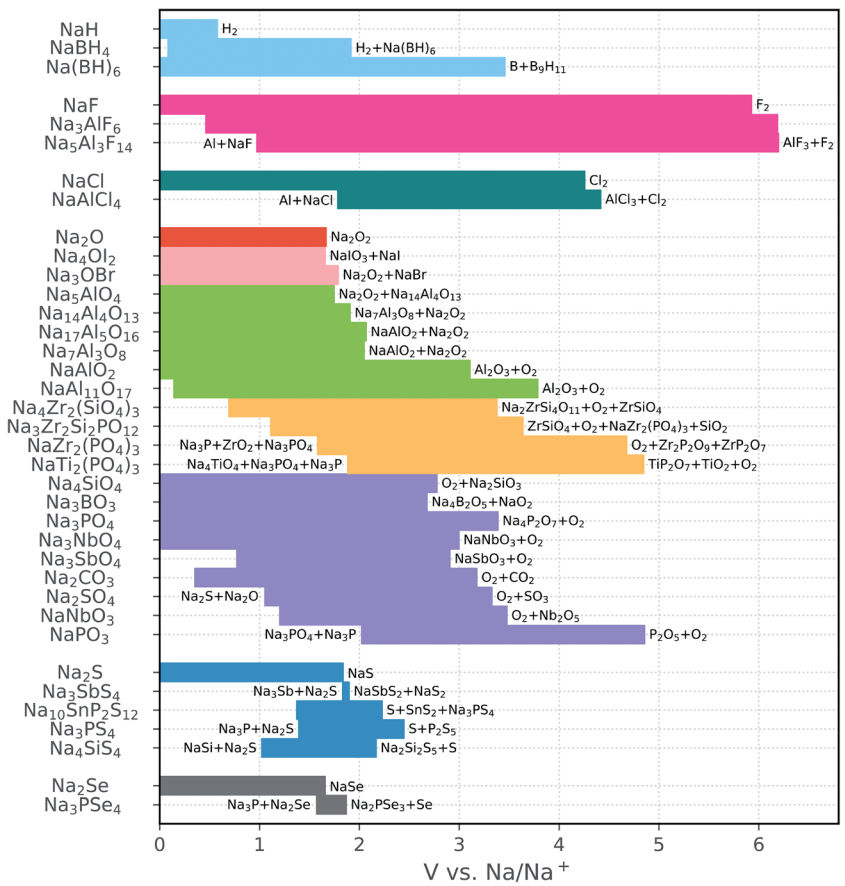

Fig. 2 Calculated electrochemical stability windows of Na solid-state electrolyte candidates. Some oxidation reactions and reduction reactions against Na metal are reported (see Table S1† for a complete list). The compounds are grouped by anion (the binaries are included for reference); the different oxide subgroups are distinguished by different colors.

of the chalcogenides is stable against Na metal, in agreement with previous reports.[14,15,37] Moreover, a reduction product of the phosphorus selenides and sulfides is Na_3P, which is a mixed ionic and electronic conductor[78] and prohibits the passivation of the electrolyte. This is in contrast with Li_3P that is an electronic insulator and can therefore passivate P-containing chalcogenide conductors.

The voltage stability ranges of the oxides are much wider than those of the chalcogenides. In particular, oxides with relatively high Na content such as Na_4SiO_4, Na_3BO_3, Na_3PO_4, and Na_3SbO_4 are all stable down to 0 V *versus* Na/Na^+. The cathodic stability becomes more limited in the presence of easily reducible species, *e.g.*, C^{4+}, Sb^{5+}, or condensed polyanions such as $[PO_3]^-$ and $[NbO_3]^-$. The latter, however, boost the oxidation limits to somewhat higher voltages (3–5 V).

Among the NaSICONs, the P-containing compounds exhibit excellent anodic stability, resisting oxidation up to approximately 5 V. At low voltage, all the explored NaSICON compositions are predicted to decompose. However, we compute a much lower driving force for reduction for the pure silicate $Na_4Zr_2(SiO_4)_3$ (decomposition energy $|\Delta E| = 0.15$ eV/atom) than for the phosphates ($|\Delta E| = 0.54$ eV/atom for $NaZr_2(PO_4)_3$ and 0.86 eV/atom for $NaTi_2(PO_4)_3$). This finding is consistent with previous experimental assessments suggesting that silicates are kinetically stabilized.[45] Fig. S2† shows the relative decomposition energies as a function of the voltage *versus* Na metal. We also note that the cathodic stability of the NaSICON-type phosphates is considerably worse than that of Na_3PO_4, which is predicted to be stable. By looking at the reduction products of $NaZr_2(PO_4)_3$ and $NaTi_2(PO_4)_3$, which always involve a metal oxide and a reduced phosphide, one may deduce that the presence of a high content of Na^+ stabilizes the PO_4 group more than the transition metals do.

In contrast to the NaSICONs, the Na aluminates are thermodynamically stable against Na metal. The only exception is the β-alumina phase $NaAl_{11}O_{17}$: the 0 K enthalpy calculations indicate that this phase is unstable with respect to the decomposition into $NaAlO_2$ + Al below 0.14 V. However, the reaction energy for the β-alumina decomposition is less than 25 meV/atom. Moreover, commonly found excess sodium induces structural disorder which makes it possible that β-alumina is stabilized by the Na-ion configurational entropy at higher temperatures. The β-alumina phase is oxidized at approximately 4 V. This is the maximum anodic stability attained by the Na aluminates, whose oxidation voltage progressively shifts to lower potentials with increasing Na content, approaching the limit of the sodium oxide binary. The antiperovskites Na_4OI_2 and Na_3OBr also have oxidation limits close to that of the Na_2O binary, consistent with the presence of fully reduced anions in all of these structures. In contrast, the borohydrides are characterized by remarkable covalent stabilization with respect to the NaH binary: the oxidation voltage increases from 0.58 V for NaH to 3.46 V for $Na_2B_{12}H_{12}$. The latter is also stable in contact with Na metal.

3.2.2 Kinetic anodic voltage limit. In our analysis, the thermodynamic anodic limit is calculated as the voltage (the Na chemical potential) at which the electrolyte is expected to decompose into other phases, accompanied by Na extraction. Such decomposition into distinct phases may not always be possible at RT until a sufficient driving force for the reaction is achieved at higher potentials. Tian *et al.*[14] defined the absolute limit of kinetic stabilization as the voltage at which Na is extracted topotactically from the electrolyte. This kinetic limit is shown for a few compounds in Table 2. As anticipated, the predicted kinetic voltage limit is always higher than the thermodynamic one, and the real anodic potential is expected to fall in between these two extremes. Large Na extraction voltages hint at the potential for substantial kinetic stabilization, especially for sodium borohydride $NaBH_4$, whose computed voltage for Na extraction is more than twice the thermodynamic anodic voltage limit.

3.3 Chemical reactivity at the cathode/electrolyte interface

Using eqn (3), we calculated the maximum driving force for the reaction between the solid-state electrolytes and different cathodes. Positive electrodes such as common layered TM oxides (TM = Cr, Mn, Fe, Co)[79] and fluorine-doped vanadium phosphates[80,81] were considered in both fully discharged and half-charged (*i.e.*, more oxidizing) states. Fig. 3 presents heat maps of the corresponding predicted reaction energies. The energy values and reaction products are listed in Tables S2–S5 of the ESI.†

We first consider the chemical reactivity against layered TM oxides. All the P-containing chalcogenide electrolytes are predicted to undergo O for Se/S anion exchange, in agreement with previous reports.[12,13,15] However, the predicted reaction products may slightly vary because of differences in datasets used to construct the high-dimensional phase diagrams. For instance, Tang *et al.*[15] predicted that the reaction at the $Na_3PS_4/NaCrO_2$ interface would produce Na_3PO_4 + $NaCrS_2$, whereas we predict Na_3PSO_3 to be an additional intermediate phase, similar to the findings of Tian *et al.*[14]

In line with ref. 14 and 15, the substitution of P with other cations (*e.g.*, Si and Sb) in the conductor generally improves the chemical stability of the interface with the TM oxide cathodes:

Table 2 Thermodynamic electrochemical window of selected solid-state electrolytes and corresponding Na extraction voltage, which sets the kinetic upper limit for oxidation

	Thermodynamic window (V)	Kinetic limit (V)
Na_3PSe_4	1.57–1.87	2.75[a]
Na_3PS_4	1.39–2.45	3.05[a]
Na_3SbS_4	1.83–1.90	3.22
$Na_{10}SnP_2S_{12}$	1.37–2.23	2.68
$NaZr_2(PO_4)_3$	1.58–4.68	4.78
$Na_4Zr_2(SiO_4)_3$	0.69–3.38	4.13
$NaAl_{11}O_{17}$	0.14–3.79	4.79
$NaAlCl_4$	1.78–4.42	4.84
Na_3AlF_6	0.46–6.19	6.35
$NaBH_4$	0.02–2.07	4.91
$Na_2B_{12}H_{12}$	0.00–3.46	4.31

[a] Data from ref. 14.

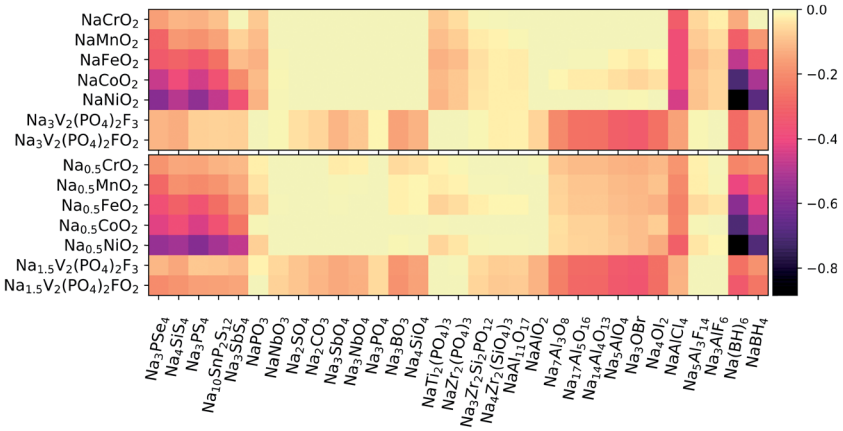

Fig. 3 Heat map of the maximum reaction energies between solid-state electrolytes and positive electrodes in both fully discharged (top) and half-charged (bottom) states. The color-bar units are eV/atom.

by switching from Na_3PS_4 to Na_3SbS_4, the reaction energies decrease by approximately 40–90% against the fully discharged TM oxide cathodes and by ~20–50% against the half-charged cathodes. In moving from the early to the late TMs in the cathode (Cr → Ni), an increasing tendency toward TM reduction by the chalcogen anions is observed. In contrast to the chalcogenides, the oxide electrolytes display negligible (*i.e.*, $|\Delta E| < 25$ meV/atom) or rather low reaction energies. Among the oxides, the most reactive interfaces are those of the Na-rich aluminates and antiperovskites against the half-charged cathodes; however, the breakdown energies $|\Delta E|$ are still lower than 150 meV/atom and thus much lower than the $|\Delta E|$ values of up to 580 meV/atom calculated for the chalcogenides. The chloride $NaAlCl_4$ behaves quite differently from the fluorides Na_3AlF_6 and $Na_5Al_3F_{14}$. In fact, whereas Cl^- is easily oxidized to Cl^{4+} and/or displaced into TM-based compounds, the fluorides are much less reactive: $|\Delta E|$ is on the order of 10–80 meV/atom, to be compared with ~200–300 meV/atom for the chloride. Finally, the borohydrides are confirmed to be strong reducing agents, especially when coupled with Co- and Ni-containing cathodes. Overall, $NaCrO_2$ appears to be the TM oxide that is most widely compatible with the different types of electrolytes. Experimental findings by Tian *et al.*[14] support this conclusion for pairings with Na_3PX_4 (X = S, Se) electrolytes.

Polyanionic cathodes such as fluorophosphates appear to be somewhat compatible with various solid-state electrolytes, including sulfides and selenides. Among the oxides, NaSICON electrolytes are particularly stable against vanadium fluorophosphate cathodes. Some reactivity ($|\Delta E| \approx$ 50–80 meV/atom) is predicted only for the Si-containing NaSICONs in contact with the partially desodiated electrodes, whose average potential (~3.5 V *vs.* Na/Na^+) is close to the intrinsic oxidation limits of such electrolytes (see Fig. 2). We also predict fairly low reactivity for $NaAl_{11}O_{17}$ ($|\Delta E| \approx$ 50 and 70 meV/atom against discharged and half-charged cathodes, respectively), whereas aluminates with higher Na content show an increasing driving force for chemical reactions, which is consistent with their lowered anodic stability limit (Fig. 2). The halo-aluminates are relatively stable against the fluorophosphate cathodes, particularly the fluorides Na_3AlF_6 and $Na_5Al_3F_{14}$ which are substantially inert ($|\Delta E| <$ 10 meV/atom). The borohydrides instead react by reducing P^{5+} to P^{3-} and releasing protons or H_2.

4 Discussion

With the discovery of numerous solid-state ion conductors that have conductivities capable of competing with those of liquid electrolytes, the critical issue for the development of SSB devices has shifted to achieving optimal (electro)chemical compatibility at the interfaces. The thermodynamic stability of these interfaces can be evaluated by construction of (grand potential) phase diagrams based on DFT calculations. The predictive capability and scalability of this approach has been demonstrated in previous work examining a wide range of chemical systems relevant for Li SSBs.[11–13] In the field of Na SSBs, computational and experimental investigations have mainly focused on chalcogenide electrolytes and their interactions with the electrodes, also providing insight into important kinetic effects.[14,15]

In this work, we have extended the previous analysis to consider a wide selection of Na solid-state electrolytes and coating candidates. In line with the literature, we find that the chalcogenide conductors exhibit poor chemical and electrochemical stabilities. The oxides display much larger voltage stability windows and generally lower reactivity against the cathode. Comparison of the calculated thermodynamic stability windows for polyanionic Na and Li compounds (see Fig. S3†) reveals two substantial differences. The first difference is that the cathodic (reduction) limits against Na/Na^+ are lower than those for similar lithiated materials, with several Na polyanion compounds being stable against Na metal. For instance, Na_3PO_4, Na_4SiO_4, and $NaAlO_2$ are all stable down to 0 V *versus* Na/Na^+, whereas the corresponding lithiated compounds are reduced at 0.74, 0.26, and 0.15 V against Li/Li^+, respectively. The other difference is that the anodic (oxidation) voltage limits of the Li compounds are generally higher than those of the Na compounds. While these observations are consistent with the standard redox potential of Na being higher than that of Li,

significant structural effects can modify this expectation. For example, the higher compatibility of Na^+ with very large anions such as I^-, Br^- or $[B_{12}H_{12}]^{2-}$ stabilizes the corresponding electrolyte structures and raises their oxidation potentials with respect to the equivalent Li compounds. In addition, by considering pairs such as MPO_3/M_3PO_4 or $MNbO_3/M_3NbO_4$ (M = Li, Na), we observe that with increasing alkali chemical potential μ_M (and content), both Na and Li compounds exhibit improved cathodic stability but reduced anodic stability. The latter is problematic as high alkaline content seems to correlate with high ionic conductivity.

The lower reducing capability of Na (*vs.* Li) broadens the selection of stable electrolyte/anode interfaces that are predicted to have either no decomposition or a very small driving force for reduction by Na. These interfaces are type A interfaces according to the classification scheme proposed by Wenzel *et al.*[82] and later adopted by Zhu *et al.*,[13] and in our analysis they are primarily formed by some oxides and borohydrides. Among the oxides, Tang *et al.*[15] identified binaries such as Sc_2O_3, ZrO_2, and HfO_2 as promising coating materials for the anode. To these materials, we add Na-based ternaries such as Na_3PO_4, Na_3NbO_4, and Na_4SiO_4, antiperovskites, and aluminum oxides. The Na aluminum oxides, in particular, are remarkably stable against reduction by Na metal, whereas Li aluminates in contact with Li metal have Al reduced and form Li–Al alloys (see Fig. S3†).

Somewhat surprisingly, the stability of the $[SiO_4]^{4-}$ and $[PO_4]^{3-}$ groups in contact with Na metal as observed in the ternary salts Na_4SiO_4 and Na_3PO_4 does not hold for the NaSICONs: our results indicate that no composition is thermodynamically stable against Na metal, which reduces the polyanions when they are in a structure with Zr or Ti metal. The presence of these TM ions providing charge compensation for the polyanions instead of Na^+ diminishes the sodium content of the NaSICONs and the lower Na content appears to correlate with a diminished cathodic stability. Likewise, pure phosphate NaSICONs are less stable against Na metal than Si-containing NaSICONs whose chemistry allows for a higher Na content. The interphase products Na_3P and NaSi (see Table S1†) provide mixed electronic and ionic conduction, matching the NaSICON/Na pair with interfaces of type B according to the classification scheme of Wenzel *et al.*[82] The simultaneous ion and electron transport provided by these reaction products can lead to the progressive consumption of the solid-state electrolyte.

The interfaces generated by decomposition of most of the chalcogenides against Na metal are also type B interfaces (Table S1†). In contrast, the electronically insulating and therefore passivating interphases Li_3P and Li_2S produced by reduction of lithium thiophosphates against Li constitute interfaces of type C. This difference points towards the use of oxides that are stable in contact with Na metal as protective layers to enable Na metal cycling. An example of an eligible anode coating candidate is orthophosphate Na_3PO_4. Indeed, the higher ionic character of the covalent bonds between phosphorus and oxygen, as compared to P–S or P–Se, widens the calculated energy gap of Na_3PO_4 ($E_g = 4.01$ eV) and prevents its reduction by Na metal, in contrast to the analogous chalcogenides Na_3PS_4 ($E_g = 2.68$ eV) and Na_3PSe_4 ($E_g = 1.56$ eV). Moreover, Na_3PO_4 displays a very low driving force for the reaction with superionic conductors such as Na_3PS_4 ($|\Delta E| \leq 20$ meV/atom), Na_3PSe_4 ($|\Delta E| \leq 17$ meV/atom) or Na_3SbS_4 (no reaction predicted). Hence, the combination of $Na/Na_3PO_4/Na_3PS_4$ may allow stable cycling of Na metal, with the thiophosphate undergoing only minimal anion-exchange reactions at the interface with the buffer layer (the calculated reaction energy is <25 meV/atom). In addition, the use of Na-containing protective oxides instead of the Na-free binaries suggested by Tang *et al.*[15] should, in principle, provide better diffusion of Na^+ through the buffer.

Because the cations in the electrolytes are fully oxidized, the anodic limits are typically controlled by oxidation of the anion. In general, higher anion electronegativity correlates with a larger oxidation voltage. This trend explains the excellent stability of fluorides (>6 V) and poor performance of sulfides and selenides, whose oxidative breakdown is predicted to occur well before 3 V *vs.* Na/Na^+. The oxides show remarkable variability in terms of anodic stability. Structures governed mainly by ionic interactions, such as the antiperovskites, display somewhat low oxidation limits, comparable to that of the simple binary oxide Na_2O. The oxidation limit increases in polyanionic compounds by virtue of the covalent interaction of the highly electronegative O with main group elements such as P, Si or B. As suggested by the parallel with the molecular orbital theory, this covalent bonding lowers the energy of the valence states and protects them from oxidation. Exemplary cases include the phosphates $NaPO_3/Na_3PO_4$ and the NaSICONs. The latter also benefit from the positive Madelung potential exerted by Ti^{4+} and Zr^{4+} on the polyanion, which further opposes the anion oxidation. The covalent stabilization of the valence states is most dramatically observed when comparing the binary NaH with the borohydrides, particularly the borane $Na_2B_{12}H_{12}$, where the B–B skeletal bonding that builds up the $[B_{12}H_{12}]^{2-}$ cluster framework results in extended electron delocalization.[83–85] For the borohydrides, the anodic stability can also be greatly enhanced by kinetic factors, as indicated by the calculated potential for desodiation. If superionic conduction could be achieved at RT, *e.g.*, by doping $NaBH_4$ into $Na_2B_{12}H_{12}$, the borane would become an eligible electrolyte candidate for SSBs.

Among the positive electrodes, the fluorophosphates show good chemical compatibility with a wide range of solid electrolytes. In fact, the fluorophosphates display limited reactivity even with the chalcogenides. Sulfides and selenides are highly reactive in contact with Co and Ni layered oxides and would be progressively consumed by the formation of interphases with a metallic character, *e.g.*, Co_3Se_4 (ref. 86) or Ni_3S_2 (ref. 87) (type B interfaces), thereby requiring the application of a buffer layer. Again, similar to the electrolyte/Na anode interface, a viable solution could be the use of Na_3PO_4 (or $NaPO_3$) as a cathode coating.

NaSICON ceramics and Na-β-alumina are the Na superionic conductors with the highest resilience to variations in cathode chemistry, forming essentially stable interfaces with all the positive electrodes considered here. Na-β(β″)-alumina is also stable against sodium metal and can now be processed into flexible ceramic membranes (≤50 μm),[88] which makes it usable as a solid-state electrolyte separator for stable Na metal cycling in

a full solid-state cell. Using NaSICON ceramics instead of Na-β-alumina would enable the working potential of the SSB to be increased if a compositional gradient from silicate (stable at low voltage) to phosphate (at high voltage) could be implemented or if the two electrolytes could be combined in a single cell. However, the high co-sintering temperatures currently needed to deliver highly conductive NaSICONs impose serious processing challenges. Finally, concerning the cathode composite, our results suggest the possibility of combining a high-energy-density cathode such as $Na_3V_2(PO_4)_2FO_2$ (ref. 81) with a fast ionic conductor such as Na_3PS_4, provided that a protective buffer layer (*e.g.*, Na_3PO_4 or $NaPO_3$) is applied. Given that chalcogenides are notably characterized by a higher degree of plasticity than oxides, this solution would ensure interparticle contact in addition to efficient ionic and electronic transport at the positive electrode, thus completing an optimized full solid-state cell design.

5 Conclusion

We have addressed the question of interfacial stability in solid-state sodium batteries by assessing the electrochemical stability and thermodynamic phase equilibria of numerous potential solid-state electrolyte/electrode combinations using DFT calculations. In addition, a direct comparison between Na- and Li-containing materials revealed differences in electrochemical behavior which are critical for tailoring the design of SSBs. More specifically, we observed that Na compounds generally display lower reduction and oxidation potentials than their Li counterparts. The enhanced cathodic stability of Na-based oxides provides multiple options to enable stable Na metal cycling, including their use as buffer layers to protect chalcogenide conductors from reduction or their direct use as solid-state electrolytes (*e.g.*, Na-β-alumina). On the other hand, the anodic stability of sodium compounds can be improved over their lithium equivalents by structure stabilization factors such as the higher compatibility of Na^+ with large anions, *e.g.*, I^- or $[B_{12}H_{12}]^{2-}$. High voltage stability (>4–5 V) was predicted for sodium halides and oxides (especially phosphate NaSICONs), and the borohydride superionic conductor $Na_2B_{12}H_{12}$ where covalent stabilization plays a major role. Finally, we identified several promising electrolyte/cathode combinations, demonstrating, among other things, the limited chemical reactivity of the layered TM oxide $NaCrO_2$ and polyanionic fluorophosphate cathodes with many potential solid electrolytes. Our findings will provide valuable guidance for the effective design of future solid-state sodium batteries as well as other technologically relevant electrochemical systems.

Conflicts of interest

There are no conflicts to declare.

Disclaimers

This document was prepared as an account of work sponsored by the United States Government. While this document is believed to contain correct information, neither the United States Government nor any agency thereof, nor the Regents of the University of California, nor any of their employees, makes any warranty, express or implied, or assumes any legal responsibility for the accuracy, completeness, or usefulness of any information, apparatus, product, or process disclosed, or represents that its use would not infringe privately owned rights. Reference herein to any specific commercial product, process, or service by its trade name, trademark, manufacturer, or otherwise, does not necessarily constitute or imply its endorsement, recommendation, or favoring by the United States Government or any agency thereof, or the Regents of the University of California. The views and opinions of authors expressed herein do not necessarily state or reflect those of the United States Government or any agency thereof or the Regents of the University of California.

Copyright notice

Acknowledgements

The Authors thank the Samsung Advanced Institute of Technology for their funding of this research. This work used resources of the National Energy Research Scientific Computing Center (NERSC), a U.S. Department of Energy Office of Science User Facility operated under Contract No. DE-AC02-05CH11231. We used also computational resources from the Extreme Science and Engineering Discovery Environment (XSEDE), which is supported by National Science Foundation grant number ACI-1548562.

References

1 H. Aono, E. Sugimoto, Y. Sadaoka, N. Imanaka and G. Adachi, Ionic Conductivity of Solid Electrolytes Based on Lithium Titanium Phosphate, *J. Electrochem. Soc.*, 1990, **137**(4), 1023–1027.
2 J. W. Fergus, Ion transport in sodium ion conducting solid electrolytes, *Solid State Ionics*, 2012, **227**, 102–112.
3 S. Ohta, T. Kobayashi and A. Takahiko, "High lithium ionic conductivity in the garnet-type oxide Li7−X La3(Zr2−X, NbX)O12 (X = 0–2), *J. Power Sources*, 2011, **196**(6), 3342–3345.
4 V. Thangadurai, D. Pinzaru, S. Narayanan and A. K. Baral, Fast Solid-State Li Ion Conducting Garnet-Type Structure Metal Oxides for Energy Storage, *J. Phys. Chem. Lett.*, 2015, **6**(2), 292–299.
5 N. Kamaya, *et al.*, A lithium superionic conductor, *Nat. Mater.*, 2011, **10**(9), 682–686.

6 Y. Seino, T. Ota, K. Takada, A. Hayashi and M. Tatsumisago, A sulphide lithium super ion conductor is superior to liquid ion conductors for use in rechargeable batteries, *Energy Environ. Sci.*, 2014, **7**(2), 627–631.
7 A. Hayashi, K. Noi, A. Sakuda and M. Tatsumisago, Superionic glass-ceramic electrolytes for room-temperature rechargeable sodium batteries, *Nat. Commun.*, 2012, **3**, 856.
8 S.-H. Bo, Y. Wang, J. C. Kim, W. D. Richards and G. Ceder, Computational and Experimental Investigations of Na-Ion Conduction in Cubic Na3PSe4, *Chem. Mater.*, 2016, **28**(1), 252–258.
9 A. Sakuda, A. Hayashi and M. Tatsumisago, "Interfacial Observation between LiCoO2 Electrode and Li2S−P2S5 Solid Electrolytes of All-Solid-State Lithium Secondary Batteries Using Transmission Electron Microscopy, *Chem. Mater.*, 2010, **22**(3), 949–956.
10 K. H. Kim, *et al.*, Characterization of the interface between LiCoO2 and Li7La3Zr2O12 in an all-solid-state rechargeable lithium battery, *J. Power Sources*, 2011, **196**(2), 764–767.
11 Y. Zhu, X. He and Y. Mo, Origin of Outstanding Stability in the Lithium Solid Electrolyte Materials: Insights from Thermodynamic Analyses Based on First-Principles Calculations, *ACS Appl. Mater. Interfaces*, 2015, **7**(42), 23685–23693.
12 W. D. Richards, L. J. Miara, Y. Wang, J. C. Kim and G. Ceder, Interface Stability in Solid-State Batteries, *Chem. Mater.*, 2016, **28**(1), 266–273.
13 Y. Zhu, X. He and Y. Mo, "First principles study on electrochemical and chemical stability of solid electrolyte–electrode interfaces in all-solid-state Li-ion batteries, *J. Mater. Chem. A*, 2016, **4**(9), 3253–3266.
14 Y. Tian, *et al.*, Compatibility issues between electrodes and electrolytes in solid-state batteries, *Energy Environ. Sci.*, 2017, **10**(5), 1150–1166.
15 H. Tang, *et al.*, Probing Solid–Solid Interfacial Reactions in All-Solid-State Sodium-Ion Batteries with First-Principles Calculations, *Chem. Mater.*, 2018, **30**(1), 163–173.
16 Y. Mo, S. P. Ong and G. Ceder, First Principles Study of the $Li_{10}GeP_2$ S_{12} Lithium Super Ionic Conductor Material, *Chem. Mater.*, 2012, **24**(1), 15–17.
17 S. P. Ong, L. Wang, B. Kang and G. Ceder, "Li−Fe−P−O2 Phase Diagram from First Principles Calculations, *Chem. Mater.*, 2008, **20**(5), 1798–1807.
18 S. P. Ong, *et al.*, Python Materials Genomics (pymatgen): A robust, open-source python library for materials analysis, *Comput. Mater. Sci.*, 2013, **68**, 314–319.
19 F. Karlsruhe, Inorganic Crystal Structure Database, available: https://icsd.fiz-karlsruhe.de.
20 G. Hautier, C. Fischer, V. Ehrlacher, A. Jain and G. Ceder, Data Mined Ionic Substitutions for the Discovery of New Compounds, *Inorg. Chem.*, 2011, **50**(2), 656–663.
21 J. P. Perdew, K. Burke and M. Ernzerhof, Generalized Gradient Approximation Made Simple, *Phys. Rev. Lett.*, 1996, **77**(18), 3865–3868.
22 G. Kresse and J. Hafner, Ab initio molecular dynamics for liquid metals, *Phys. Rev. B: Condens. Matter Mater. Phys.*, 1993, **47**(1), 558–561.
23 P. E. Blöchl, Projector augmented-wave method, *Phys. Rev. B: Condens. Matter Mater. Phys.*, 1994, **50**(24), 17953–17979.
24 V. I. Anisimov, J. Zaanen and O. K. Andersen, Band theory and Mott insulators: Hubbard U instead of Stoner I, *Phys. Rev. B: Condens. Matter Mater. Phys.*, 1991, **44**(3), 943–954.
25 A. Jain, *et al.*, Formation enthalpies by mixing GGA and GGA+U calculations, *Phys. Rev. B: Condens. Matter Mater. Phys.*, 2011, **84**(4), 045115.
26 L. Wang, T. Maxisch and G. Ceder, Oxidation energies of transition metal oxides within the GGA+U framework, *Phys. Rev. B: Condens. Matter Mater. Phys.*, 2006, **73**(19), 195107.
27 O. Kubaschewski, C. B. Alcock and P. J. Spencer, *Materials Thermochemistry*, Pergamon Press, Oxford, 6th edn, 1993.
28 M. W. J. Chase, *NIST-JANAF Thermochemical Tables*, American Chemical Society, Washington, DC, 4th edn, 1998, American Institute of Physics for the National Institute of Standards and Technology, New York, 1998.
29 G. Hautier, S. P. Ong, A. Jain, C. J. Moore and G. Ceder, Accuracy of density functional theory in predicting formation energies of ternary oxides from binary oxides and its implication on phase stability, *Phys. Rev. B: Condens. Matter Mater. Phys.*, 2012, **85**(15), 155208.
30 Y.-F. Y. Yao and J. T. Kummer, Ion exchange properties of and rates of ionic diffusion in beta-alumina, *J. Inorg. Nucl. Chem.*, 1967, **29**(9), 2453–2475.
31 D. Kundu, E. Talaie, V. Duffort and L. F. Nazar, The Emerging Chemistry of Sodium Ion Batteries for Electrochemical Energy Storage, *Angew. Chem., Int. Ed.*, 2015, **54**(11), 3431–3448.
32 Z. Wen, Y. Hu, X. Wu, J. Han and Z. Gu, Main Challenges for High Performance NAS Battery: Materials and Interfaces, *Adv. Funct. Mater.*, 2013, **23**(8), 1005–1018.
33 H. Sakaebe, ZEBRA Batteries, in *Encyclopedia Of Applied Electrochemistry*, Springer, New York, NY, 2014, pp. 2165–2169.
34 T. Oshima, M. Kajita and A. Okuno, Development of Sodium-Sulfur Batteries, *Int. J. Appl. Ceram. Technol.*, 2004, **1**(3), 269–276.
35 C. Beevers and M. Ross, The Crystal Structure of "Beta Alumina" Na2O·11Al2O3, *Z. für Kristallogr. - Cryst. Mater.*, 1937, **97**(1–6), 59–66.
36 J. Thery and D. Briançon, Chimie minérale-sur les propriétés d'un nouvel aluminate de sodium NaAl5O8, *C. R. Acad. Sci.*, 1962, **254**, 2782.
37 S. Wenzel, T. Leichtweiss, D. A. Weber, J. Sann, W. G. Zeier and J. Janek, Interfacial Reactivity Benchmarking of the Sodium Ion Conductors Na_3PS_4 and Sodium β-Alumina for Protected Sodium Metal Anodes and Sodium All-Solid-State Batteries, *ACS Appl. Mater. Interfaces*, 2016, **8**(41), 28216–28224.
38 M. G. Barker, P. G. Gadd and S. C. Wallwork, A new sodium aluminate Na17Al5O16, *J. Chem. Soc., Chem. Commun.*, 1982, (9), 516–517.

39 B. Shen, *et al.*, Improved electrochemical performance of NaAlO2-coated LiCoO2 for lithium-ion batteries, *J. Solid State Electrochem.*, 2017, **21**(4), 1195–1201.
40 H. Y.-P. Hong, "Crystal structures and crystal chemistry in the system Na1+xZr2SixP3−xO12, *Mater. Res. Bull.*, 1976, **11**(2), 173–182.
41 J. B. Goodenough, H. Y.-P. Hong and J. A. Kafalas, Fast Na+-ion transport in skeleton structures, *Mater. Res. Bull.*, 1976, **11**(2), 203–220.
42 S. Chen, *et al.*, Challenges and Perspectives for NASICON-Type Electrode Materials for Advanced Sodium-Ion Batteries, *Adv. Mater.*, 2017, **29**(48), 1700431.
43 U. Von Alpen, M. F. Bell and H. H. Höfer, Compositional dependence of the electrochemical and structural parameters in the Nasicon system (Na1+xSixZr2P3−xO12), *Solid State Ionics*, 1981, **3**, 215–218.
44 W. Zhou, Y. Li, S. Xin and J. B. Goodenough, Rechargeable Sodium All-Solid-State Battery, *ACS Cent. Sci.*, 2017, **3**(1), 52–57.
45 K. D. Kreuer and U. Warhus, NASICON solid electrolytes, *Mater. Res. Bull.*, 1986, **21**(3), 357–363.
46 J. Zhu, *et al.*, Sodium Ion Transport Mechanisms in Antiperovskite Electrolytes Na3OBr and Na4OI2: An in Situ Neutron Diffraction Study, *Inorg. Chem.*, 2016, **55**(12), 5993–5998.
47 Y. Wang, *et al.*, Structural manipulation approaches towards enhanced sodium ionic conductivity in Na-rich antiperovskites, *J. Power Sources*, 2015, **293**, 735–740.
48 M. D. Leblanc, U. M. Gundusharma and E. A. Secco, Electrical conductivity of superionic solid solutions of Na_2SO_4 with Mx (XO_4)y -[M=Na, K, Rb, Cd, Gd and X=W, Mo, S, Si;x=1, 2, 4 andy=1, 3], *Solid State Ionics*, 1986, **20**(1), 61–68.
49 J. T. S. Irvine and A. R. West, Sodium ion-conducting solid electrolytes in the system Na_3PO_4-Na_2SO_4, *J. Solid State Chem.*, 1987, **69**(1), 126–134.
50 H. Hruschka, E. Lissel and M. Jansen, Na-Ion conduction in the solid solutions of Na3PO4/Na2SO4 and Na3AlF6/Na2SO4, *Solid State Ionics*, 1988, **28**, 159–162.
51 M. Pompetzki, R. E. Dinnebier and M. Jansen, Sodium dithiophosphate(V): Crystal structure, sodium ionic conductivity and dismutation, *Solid State Sci.*, 2003, **5**(11–12), 1439–1444.
52 M. Jansen and U. Henseler, Synthesis, structure determination, and ionic conductivity of sodium tetrathiophosphate, *J. Solid State Chem.*, 1992, **99**(1), 110–119.
53 N. Tanibata, K. Noi, A. Hayashi and M. Tatsumisago, Preparation and characterization of highly sodium ion conducting Na3PS4-Na4SiS4 solid electrolytes, *RSC Adv.*, 2014, **4**(33), 17120–17123.
54 A. Banerjee, *et al.*, Na_3SbS_4: A Solution Processable Sodium Superionic Conductor for All-Solid-State Sodium-Ion Batteries, *Angew. Chem.*, 2016, **128**(33), 9786–9790.
55 W. D. Richards, *et al.*, Design and synthesis of the superionic conductor Na10SnP2S12, *Nat. Commun.*, 2016, **7**, 11009.
56 T. J. Udovic, *et al.*, Sodium superionic conduction in Na2B12H12, *Chem. Commun.*, 2014, **50**(28), 3750–3752.
57 M. Matsuo, Y. Nakamori, S. Orimo, H. Maekawa and H. Takamura, Lithium superionic conduction in lithium borohydride accompanied by structural transition, *Appl. Phys. Lett.*, 2007, **91**(22), 224103.
58 K. Takahashi, *et al.*, All-solid-state lithium battery with LiBH4 solid electrolyte, *J. Power Sources*, 2013, **226**, 61–64.
59 D. M. F. Santos and C. A. C. Sequeira, Sodium borohydride as a fuel for the future, *Renewable Sustainable Energy Rev.*, 2011, **15**(8), 3980–4001.
60 Z. Lu and F. Ciucci, Metal Borohydrides as Electrolytes for Solid-State Li, Na, Mg, and Ca Batteries: A First-Principles Study, *Chem. Mater.*, 2017, **29**(21), 9308–9319.
61 B. L. Ellis and L. F. Nazar, Sodium and sodium-ion energy storage batteries, *Curr. Opin. Solid State Mater. Sci.*, 2012, **16**(4), 168–177.
62 S. Ha, J.-K. Kim, A. Choi, Y. Kim and K. T. Lee, "Sodium–Metal Halide and Sodium–Air Batteries, *ChemPhysChem*, 2014, **15**(10), 1971–1982.
63 S. Bhavaraju, A. V. Joshi, M. Robins and A. Eccleston, Intermediate temperature sodium-metal halide battery, US9537179B2, 25-Sep-2014.
64 D. R. Spearing, J. F. Stebbins, and I. Farnan, *Diffusion and the Dynamics of Displacive Phase Transitions in Cryolite (Na3AlF6) and Chiolite (NasAl3F14): Multi-Nuclear NMR Studies*, p. 14.
65 L. Foy and P. A. Madden, Ionic Motion in Crystalline Cryolite, *J. Phys. Chem. B*, 2006, **110**(31), 15302–15311.
66 G. Nazri, Preparation, structure and ionic conductivity of lithium phosphide, *Solid State Ionics*, 1989, **34**(1), 97–102.
67 H. Maekawa, *et al.*, Halide-Stabilized $LiBH_4$, a Room-Temperature Lithium Fast-Ion Conductor, *J. Am. Chem. Soc.*, 2009, **131**(3), 894–895.
68 I.-H. Chu, *et al.*, Room-Temperature All-solid-state Rechargeable Sodium-ion Batteries with a Cl-doped Na_3PS_4 Superionic Conductor, *Sci. Rep.*, 2016, **6**, 33733.
69 S. Ujiie, T. Inagaki, A. Hayashi and M. Tatsumisago, "Conductivity of 70Li2S·30P2S5 glasses and glass–ceramics added with lithium halides, *Solid State Ionics*, 2014, **263**, 57–61.
70 S. Zhai, L. Li, F. Chen, Q. Jiao, C. Rüssel and C. Lin, "Glass Formation and Ionic Conduction Behavior in GeSe2–Ga2Se3–NaI Chalcogenide System, *J. Am. Ceram. Soc.*, 2015, **98**(12), 3770–3774.
71 Å. Olin, *Chemical Thermodynamics of Selenium*. Elsevier, 2005.
72 S. P. Ong, *et al.*, Voltage, stability and diffusion barrier differences between sodium-ion and lithium-ion intercalation materials, *Energy Environ. Sci.*, 2011, **4**(9), 3680–3688.
73 B. M. Gallant, *et al.*, Chemical and Morphological Changes of Li–O2 Battery Electrodes upon Cycling, *J. Phys. Chem. C*, 2012, **116**(39), 20800–20805.
74 V. Viswanathan, *et al.*, Electrical conductivity in Li2O2 and its role in determining capacity limitations in non-aqueous Li-O2 batteries, *J. Chem. Phys.*, 2011, **135**(21), 214704.

75 S. Kang, Y. Mo, S. P. Ong and G. Ceder, "Nanoscale Stabilization of Sodium Oxides: Implications for Na–O2 Batteries, *Nano Lett.*, 2014, **14**(2), 1016–1020.

76 R. Tegman, The crystal structure of sodium tetrasulphide, Na_2 S_4, *Acta Crystallogr., Sect. B: Struct. Crystallogr. Cryst. Chem.*, 1973, **29**(7), 1463–1469.

77 H. Föppl, E. Busmann and F.-K. Frorath, Die Kristallstrukturen von α-Na_2S_2 und K_2S_2, β-Na_2S_2 und Na_2Se_2, *Z. Anorg. Allg. Chem.*, 1962, **314**(1–2), 12–20.

78 X. Yu, G. Giorgi, H. Ushiyama and K. Yamashita, First-principles study of fast Na diffusion in Na3P, *Chem. Phys. Lett.*, 2014, **612**, 129–133.

79 P.-F. Wang, Y. You, Y.-X. Yin and Y.-G. Guo, Layered Oxide Cathodes for Sodium-Ion Batteries: Phase Transition, Air Stability, and Performance, *Adv. Energy Mater.*, 2018, **8**(8), 1701912.

80 R. K. B. Gover, A. Bryan, P. Burns and J. Barker, The electrochemical insertion properties of sodium vanadium fluorophosphate, Na3V2(PO4)2F3, *Solid State Ionics*, 2006, **177**(17), 1495–1500.

81 M. Bianchini, P. Xiao, Y. Wang and G. Ceder, Additional Sodium Insertion into Polyanionic Cathodes for Higher-Energy Na-Ion Batteries, *Adv. Energy Mater.*, 2017, **7**(18), 1700514.

82 S. Wenzel, T. Leichtweiss, D. Krüger, J. Sann and J. Janek, "Interphase formation on lithium solid electrolytes—An in situ approach to study interfacial reactions by photoelectron spectroscopy, *Solid State Ionics*, 2015, **278**, 98–105.

83 R. Hoffmann and W. N. Lipscomb, Theory of Polyhedral Molecules. I. Physical Factorizations of the Secular Equation, *J. Chem. Phys.*, 1962, **36**(8), 2179–2189.

84 K. Wade, The structural significance of the number of skeletal bonding electron-pairs in carboranes, the higher boranes and borane anions, and various transition-metal carbonyl cluster compounds, *J. Chem. Soc., Chem. Commun.*, 1971, (15), 792–793.

85 R. B. King and D. H. Rouvray, Chemical applications of group theory and topology. 7. A graph-theoretical interpretation of the bonding topology in polyhedral boranes, carboranes, and metal clusters, *J. Am. Chem. Soc.*, 1977, **99**(24), 7834–7840.

86 W. Li, *et al.*, Hydrothermal Synthesis of Monolithic Co3Se4 Nanowire Electrodes for Oxygen Evolution and Overall Water Splitting with High Efficiency and Extraordinary Catalytic Stability, *Adv. Energy Mater.*, 2017, **7**(17), 1602579.

87 Z. W. Lu, B. M. Klein and D. J. Singh, Electronic structure of heazlewoodite Ni3S2, *Phys. Rev. B: Condens. Matter Mater. Phys.*, 1996, **54**(19), 13542–13545.

88 E. Yi, E. Temeche and R. M. Laine, "Superionically Conducting β''-Al2O3 Thin Films Processed Using Flame Synthesized Nanopowders, *J. Mater. Chem. A*, 2018, **6**, 12411–12419.